A modified motor-clutch model reveals that neuronal growth cones respond faster to soft substrates

Laura Pulido Cifuentes[a], Ahmad I. M. Athamneh[a], Yuri Efremov[b,c,h], Arvind Raman[b,c], Taeyoon Kim[d], and Daniel M. Suter[a,c,d,e,f,g,*]

[a]Department of Biological Sciences, [b]School of Mechanical Engineering, [c]Birck Nanotechnology Center, [d]Weldon School of Biomedical Engineering, [e]Purdue Institute for Integrative Neuroscience, [f]Purdue Institute for Inflammation, Immunology, and Infectious Disease, and [g]Bindley Bioscience Center, Purdue University, West Lafayette, IN 47907

[h]Institute for Regenerative Medicine, Sechenov University, Moscow 119991, Russia

ABSTRACT **Neuronal growth cones sense a variety of cues including chemical and mechanical ones to establish functional connections during nervous system development. Substrate-cytoskeletal coupling is an established model for adhesion-mediated growth cone advance; however, the detailed molecular and biophysical mechanisms underlying the mechanosensing and mechanotransduction process remain unclear. Here, we adapted a motor-clutch model to better understand the changes in clutch and cytoskeletal dynamics, traction forces, and substrate deformation when a growth cone interacts with adhesive substrates of different stiffnesses. Model parameters were optimized using experimental data from *Aplysia* growth cones probed with force-calibrated glass microneedles. We included a reinforcement mechanism at both motor and clutch level. Furthermore, we added a threshold for retrograde F-actin flow that indicates when the growth cone is strongly coupled to the substrate. Our modeling results are in strong agreement with experimental data with respect to the substrate deformation and the latency time after which substrate-cytoskeletal coupling is strong enough for the growth cone to advance. Our simulations show that it takes the shortest time to achieve strong coupling when substrate stiffness was low at 4 pN/nm. Taken together, these results suggest that *Aplysia* growth cones respond faster and more efficiently to soft than stiff substrates.**

Monitoring Editor
Stephanie Gupton
University of North Carolina
at Chapel Hill

Received: Sep 13, 2023
Revised: Feb 2, 2024
Accepted: Feb 5, 2024

SIGNIFICANCE STATEMENT

- How neuronal growth cones sense substrates of different stiffness is not well understood.
- We have modified the motor-clutch model by including reinforcement at the motor and clutch level as well as threshold for F-actin flow when strong substrate-cytoskeletal coupling occurs. We found that simulated and experimental data for latency time and substrate deformation are in strong agreement.
- Our results suggest that *Aplysia* growth cones respond faster to soft versus stiff substrates. These findings provide a framework for future experimental studies and will improve our understanding of cellular mechanosensing.

This article was published online ahead of print in MBoC in Press (http://www.molbiolcell.org/cgi/doi/10.1091/mbc.E23-09-0364) on February 14, 2024.

*Address correspondence to: Daniel M. Suter, PhD (dsuter@purdue.edu).

Abbreviations used: apCAM, *Aplysia* cell adhesion molecule; ASW, artificial sea water; C, central; CNS, Central nervous system; ConA, Concanavalin A; DIC, differential interference contrast; NMII, non-muscle myosin II; P, peripheral; PLL, poly-L-lysine; RBI, restrained bead interaction; T, transition.

INTRODUCTION

Growth cones are motile and dynamic structures at the tips of axons and dendrites, that exhibit either attractive or repulsive behaviors in response to specific diffusible or immobilized extracellular chemical (Stoeckli, 2018), mechanical (Koser *et al*., 2016), topographical (Spedden *et al*., 2014), and electrical cues (Yamashita, 2015). The growth cone continuously explores the extracellular environment to guide axon pathfinding and is critical for axon outgrowth, which is a process that was traditionally described to occur in three stages named protrusion, engorgement, and consolidation (Dent and Gertler, 2003; Lowery and Vactor, 2009). Protrusion is the extension of the growth cone edge driven by F-actin polymerization. Later engorgement occurs when microtubules (MTs) invade protrusions and transport organelles and vesicles into F-actin-rich regions. Finally, consolidation results from the contraction of the growth cone neck forming the new axon shaft and restoring the bidirectional vesicle transport.

Different models have been proposed to explain the mechanisms underlying growth cone advance, and in consequence, axon outgrowth. A recently proposed model suggests that, at least for CNS neurons in three-dimensional (3D) cultures, growth cones advance solely by an ameboid, protrusion-driven process independent of making adhesive contacts with the environment and applying traction forces (Santos *et al*., 2020). In contrast, a large body of evidence mainly from experiments conducted with two-dimensional (2D) cultures of both PNS and CNS neurons supports another model of growth cone motility and neurite growth which involves the formation of adhesions between the growth cone and immobile ligands in the extracellular matrix or on cellular surfaces (Suter and Forscher, 2000; Miller and Suter, 2018). Mitchison and Kirschner (1988) were the first to propose a mechanistic model to explain substrate-mediated growth cone advance. According to this "motor-clutch" or "substrate-cytoskeletal coupling" model, the growth cone attaches to a substrate through cell adhesion molecules (CAMs), that interact with actin filaments via specific coupling molecules (Figures 1 and 2B) and contribute to tension build up. Consequently, the adhesions "clutch" the actin retrograde flow by counteracting the myosin force and transmitting the myosin forces to the substrate.

Experimental evidence supports this model for all major types of CAMs, such as immunoglobulin superfamily CAMs, integrins, and cadherins. The first evidence came from studies using neuronal growth cones derived from the invertebrate *Aplysia californica* and probed using beads coated with the *Aplysia* cell adhesion molecule (apCAM), a homologue of the vertebrate neural cell adhesion molecule (Suter *et al*., 1998). Restraining apCAM-coated beads with a microneedle in the so-called restrained bead interaction (RBI) assay resulted in attenuation of actin flow, force build up, and growth cone advance specifically along the needle-central (C) domain axis. Similarly, in rat hippocampal neurons, a mechanical linkage was found between L1-CAM-laminin adhesions and F-actin mediated by coupling molecules shootin1a and cortactin (Abe *et al*., 2018) as well as between N-cadherin-N-cadherin adhesions and F-actin mediated by α-catenin (Bard *et al*., 2008). Not surprisingly, integrin-laminin adhesions resulted in a similar response of reduced actin retrograde flow in growth cones from *Xenopus* spinal neurons (Nichol *et al*., 2016). Several clutch or coupling proteins have been implicated in formation of a molecular clutch between adhesion receptors and F-actin including cortactin, shootin 1a, catenin, talin, vinculin, and paxillin. Moreover, the adhesion stabilization and dynamics are regulated through the activation of several signaling enzymes including focal-adhesion kinase (FAK; Robles and Gomez, 2006), Src (Suter and Forscher, 2001), and p-21 activated kinase (Pak1; Santiago-Medina *et al*., 2013; Toriyama *et al*., 2013) leading to changes in the phosphorylation status of different proteins of the adhesion complex such as paxillin and shootin1. However, while several molecular components of adhesion-mediated neurite growth have been identified, it has remained unclear how the stiffness of the adhesion substrate regulates the formation of clutches and thereby growth cone advance.

Previous studies regarding neurite outgrowth on flexible substrates have provided conflicting results about the effects of substrate stiffness on neurite growth even for the same neuronal cell type. Some studies have reported higher neurite outgrowth and branching on soft 2D substrates (Flanagan *et al*., 2002; Georges *et al*., 2006; Franze *et al*., 2009). While Kostic and colleagues (2007) and Tanaka *et al*. (2018) reported that hippocampal neurons grown on soft substrates exhibit increased neuritogenesis and neurite outgrowth, Koch and colleagues (2012) found that hippocampal neurons are insensitive to substrate stiffness (Koch *et al*., 2012; Kostic *et al*., 2007; Tanaka *et al*., 2018). Similarly, Koch and colleagues reported that dorsal root ganglion (DRG) cells exhibit maximal outgrowth on substrates of 1kPa, whereas another group found that DRG cells have a higher outgrowth on substrates of 10 kPa in comparison with softer substrates (Koch *et al*., 2012; Rosso *et al*., 2017). In summary, while there is emerging evidence that different neurons exhibit distinct mechanosensing responses, there are still significant gaps in our understanding of mechanosensing.

Computational modeling is a powerful approach to better understand cellular behavior in response to changing specific parameters and allows comparing simulation with experimental results. Chan and Odde (2008) developed a mathematical model to study the mechanosensing of substrate stiffness by cells. The model predicts two regimes: (1) "frictional slippage" occurs on stiff substrates, when clutches bind quickly to F-actin and break before many clutches are bound, resulting in low traction forces and high retrograde F-actin flow. (2) A "load and fail" regime occurs on soft substrates. It is characterized by an oscillatory behavior where substrate compliance increases the clutch-F-actin bond lifetime and allows many clutches to be bound at specific time point, contributing to the slowdown of actin retrograde flow and increase in traction force. To test this model, the researchers measured retrograde actin flow and traction force production in embryonic chick forebrain neurons growing on compliant substrates and detected a significant switch between the "frictional slippage" and "load and fail" regimes at a substrate stiffness of ~1 kPa (Chan and Odde, 2008). A detailed sensitivity analysis of various model parameters was conducted in a follow-up study by the same group, and found that the optimum stiffness is more sensitive to changes in clutch-related parameters than to motor-related parameters (Bangasser *et al*., 2013). Several studies have shown the versatility and robustness of this model by adapting it to different cell types and substrates. For example, by including talin unfolding kinetics, it was shown that the above-mentioned biphasic relationship between stiffness and traction force depends on talin depletion, and that a monotonic trend is observed between those variables when talin reinforces the integrin-actin coupling above a specific force threshold (Elosegui-Artola *et al*., 2016). Additionally, the model has successfully reproduced the effect of catch-bond kinetics, ligand spacing, and the inclusion of different integrin types with different kinetics as a mechanism for adhesion strengthening (Elosegui-Artola *et al*., 2014; Oria *et al*., 2017).

Here, we modified the motor-clutch model for mechanosensing by large *Aplysia* growth cones, which are an ideal model system for analyzing cytoskeletal dynamics and mechanics. We added several new features to the motor-clutch model. First, we introduced stiffness-dependent reinforcement at both the motor and clutch level. Second, we included two new output variables: 1) the latency time, which represents the time when the F-actin flow decays to 20 nm/s and strong coupling occurs, and 2) the substrate deformation at the latency time. Third, in contrast to previous studies, our motor-clutch model results in a stable steady state, whereas the previous model resulted in an unstable oscillating steady state. After conducting sensitivity analyses, we found that the latency time and substrate deformation are less sensitive to parameter changes at 4 pN/nm than at other substrate stiffnesses. Furthermore, we found that the latency time exhibits a biphasic behavior with respect to the substrate stiffness being the shortest at 4 pN/nm. These results suggest that 4 pN/nm could be the optimum substrate stiffness for *Aplysia* growth cones.

RESULTS

A modified motor-clutch model for growth cone advance on different substrate stiffness

To better understand how neuronal growth cones advance on adhesive substrates of different stiffness, we have adapted a previously established motor-clutch model (Chan and Odde, 2008; Bangasser *et al.*, 2013) to the *Aplysia* growth cone system (Suter *et al.*, 1998; Athamneh *et al.*, 2015; Miller and Suter, 2018). This approach allowed us not only to compare experimental with modeling data, but also to extract parameter values from experimental data for our model to make it more robust.

A growth cone has three regions based on differences in cytoskeletal structure and dynamics as well as organelle distribution (Figure 1A). The peripheral (P) domain contains both lamellipodia, that are composed of crosslinked F-actin networks, and filopodia, that consist of F-actin bundles. The transition (T) zone is located between the P domain and the C domain and is characterized by ADF-cofilin-mediated actin severing and nonmuscle myosin II (NMII)-powered contraction of the F-actin network, which leads to the formation of actin arcs. The C domain is rich in organelles and MTs. The actin filaments in lamellipodia and filopodia are constantly turned over by a combination of actin assembly along the leading edge and at filopodial tips, retrograde F-actin flow, and actin severing and disassembly in the T zone (Miller and Suter, 2018). Retrograde F-actin flow is a phenomenon found in all motile cells and largely driven by NMII activity in addition to actin assembly push against the plasma membrane and actin turn over in the T zone (Zhang *et al.*, 2003; Medeiros *et al.*, 2006; Burnette *et al.*, 2008)

The motor-clutch model used in this study is a one-dimensional model, where adhesions/clutches develop between a single filopodium and an elastic substrate (Figure 1B; Chan and Odde, 2008; Bangasser *et al.*, 2013). Friction develops between the actin filaments and bound adhesions/clutches, which slows down the rate of actin flow. Here, we consider three events affecting the state of adhesions/clutches: (1) binding of a clutch to F-actin with a constant rate k_{on} (Figure 1C), (2) force-dependent unbinding of a clutch from F-actin with a rate k_{off} (Equation 5 in *Materials and Methods* section; Figure 1D), and (3) adhesion reinforcement by adding a new clutch at a rate k_{add}, (Equation 6) when at least one of the bound clutches bears a force ≥10 pN (Figure 1E). The mechanical free body diagram of the motor-clutch model is depicted in Supplemental Figure 1. Each step of the simulation along with the variables and parameters is shown in Supplemental Figure 2 and Supplemental Tables 1 and 2. The simulation starts with an unloaded actin flow velocity of 100 nm/s under the assumption of no bound clutches. Clutches keep binding and unbinding, thereby affecting the retrograde actin flow speed v_f (Equation 7), clutch position x_i (Equation 8) and substrate position x_{sub} (Equation 9). Thus, as the simulation progresses, the actin retrograde flow contributes to tension build up on bound clutches. The bound clutches transmit the force generated by the myosin motors (n_m*F_s) to the elastic substrate with substrate stiffness defined by a spring constant (K_{sub}) and cause substrate deformation (Δx_{sub}). The simulation runs until actin flow is attenuated to 20 nm/s. This flow rate corresponds to 80% reduction of actin flow, which has been observed when *Aplysia* growth cones transition from a state of slow advance and little/no coupling on poly-L-lysine (PLL) to a state of fast advance and strong coupling on physiological substrates (Lin and Forscher, 1995; Suter *et al.*, 1998).

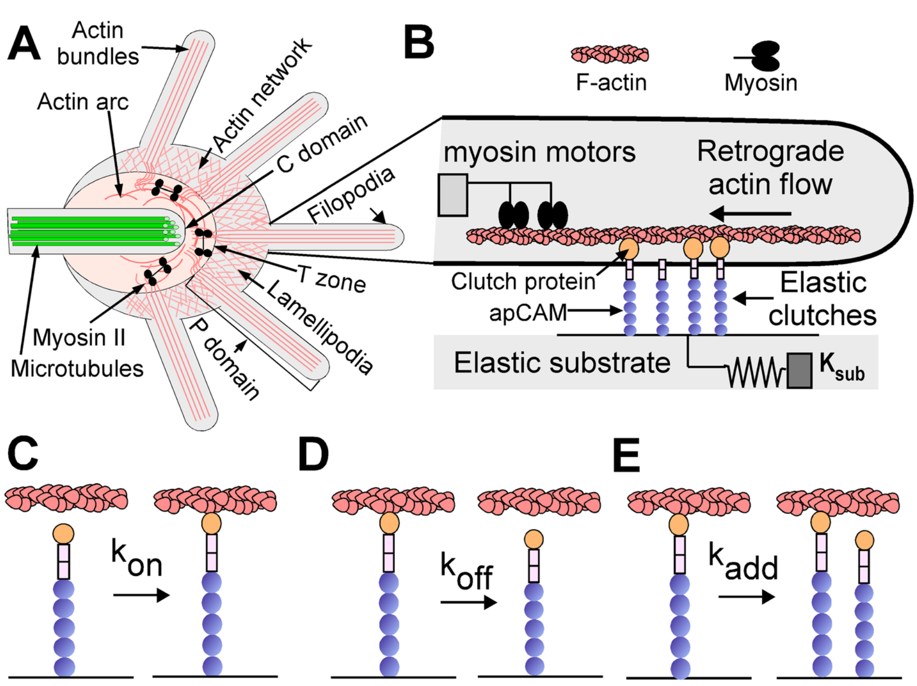

FIGURE 1: Motor-clutch model for adhesion-mediated growth cone advance. (A) Growth cone organization and cytoskeletal components. (B) Motor-clutch model components in cross-section of a single filopodia. (C) Binding of a clutch to F-actin with a constant rate k_{on}. (D) Force-dependent unbinding of a clutch from F-actin with a rate k_{off}. (E) Adhesion reinforcement event that includes the addition of a new clutch at a rate k_{add}, when at least one of the bound clutches can hold a force of 10 pN.

Parameter optimization with data derived from microneedle experiments

To optimize some of the parameters of the model, we used experimental data of adhesion-mediated growth cone advance triggered by stiffness-calibrated microneedles reported in our previous study (Athamneh *et al.*, 2015). Specifically, *Aplysia* bag cell neurons were plated on cover glass coated with PLL, and after 1 d in culture, a stiffness-calibrated microneedle coated with the

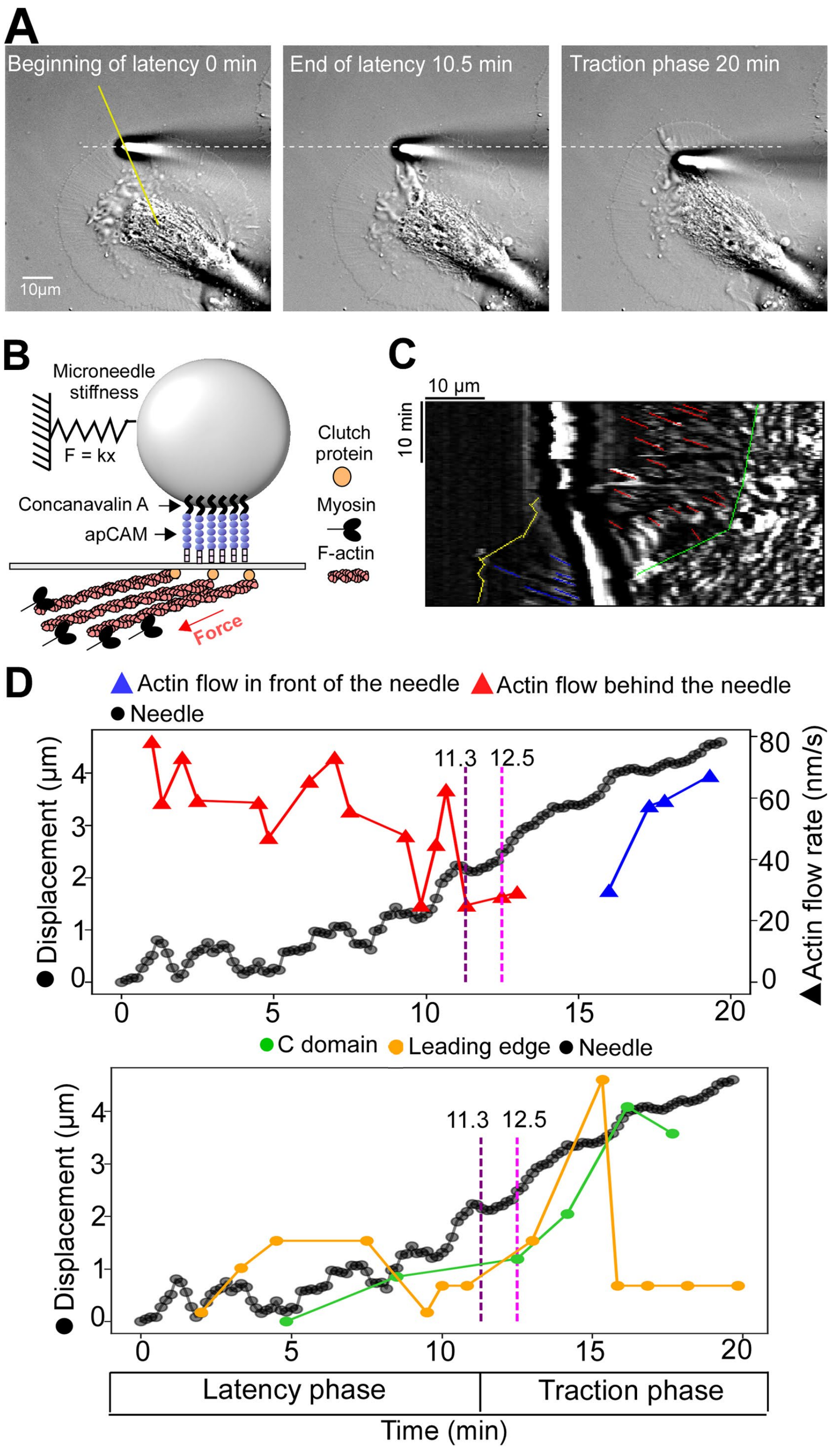

FIGURE 2: Experimental approach to study stiffness-dependent adhesion-mediated growth cone advance. (A) Different phases of adhesion-mediated *Aplysia* growth cone advance using a ConA-coated microneedle with a stiffness of 2 pN/nm (images adapted from Figure 6A of Athamneh *et al.*, 2015). (B) Schematic of the different components of the motor-clutch model in the context of the needle experiment. (C) Kymograph along the line shown in (A).
(D) Information about needle tip, C domain boundary, and leading edge displacements as well as F-actin flow rates over time obtained from kymograph shown in (C). The purple vertical line indicates the time when the retrograde actin flow is 20 nm/s, and the pink vertical line shows the time when the C domain starts to advance towards the microneedle.

lectin Concanavalin A (ConA) was placed in contact with the P domain of a growth cone (Athamneh *et al.*, 2015). The growth cone response to the ConA-coated needle was recorded by time-lapse imaging using differential interference contrast (DIC) starting with the initial contact between the growth cone and the microneedle until the C domain advanced towards the contact site with the microneedle (Figure 2). The original experimentally defined latency phase is a time range between the initial contact with the new substrate and the time point when major growth cone structural or cytoskeletal rearrangements such as C domain advance start (Suter *et al.*, 1998; Athamneh *et al.*, 2015). The following traction phase is a time range when significant myosin-generated traction force develops, and C domain and P domain advance in concert at higher velocity (Figure 2A).

Microneedle-induced advance of *Aplysia* bag cell growth cones can be mediated by both purified apCAM or by ConA (Figure 2B), a lectin previously shown to interact with apCAM among other membrane proteins (Thompson *et al.*, 1996; Suter *et al.*, 1998; Athamneh *et al.*, 2015). Based on the needle deformation and stiffness values, we were able to determine the traction force as reported in our previous study (Athamneh *et al.*, 2015). By creating kymographs along the C domain-microneedle axis (yellow line in Figure 2A), we have collected additional information in the current study (Figure 2, C and D): rates of actin retrograde flow behind (red lines) and in front of the microneedle (blue lines), as well as the displacement of the C domain boundary (green line) and of the leading edge (yellow line). Based on the kymograph analysis (Figure 2C) and in agreement with the results of the studies using the RBI assay, we found that during the latency phase, the position of the C domain boundary and leading edge do not change much, and that the retrograde actin flow behind the microneedle oscillates around 50–60 nm/s during most of the latency period. At the end of the latency period, there is a significant increase in the microneedle deformation along with a decrease in the actin flow to 20 nm/s behind the needle (purple dashed line in Figure 2D). Later, at the beginning of the traction phase, the advance of the C domain boundary and leading edge to the adhesion site was observed (Figure 2D; pink dashed line), suggesting that the substrate-cytoskeleton coupling has been strengthened to a level when major cytoskeletal rearrangements occur (Suter *et al.*, 1998). We also measured actin flow rates in the advancing P domain in front

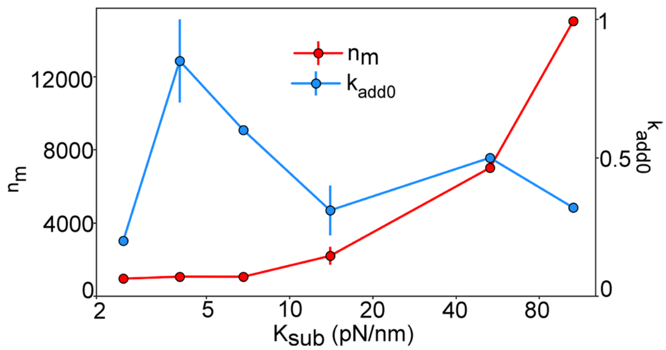

FIGURE 3: Parameter optimization. Optimized number of motors and reinforcement constants at different substrate stiffness. The number of motors (n_m) and the initial reinforcement rate (k_{add0}), were optimized for each available experiment at a specific substrate stiffness. The number of experiments used for the optimization was $n = 2$ for 2.5 pN/nm, 4 pN/nm, and 14 pN/nm, and $n = 1$ for the rest of substrate stiffnesses. Thus, for the substrate stiffness with $n = 2$, the filled circles correspond to the average of the average of simulations optimized with each experiment, and the bars corresponds to the SD. x-axis is shown on a $\log_{10}$ scale.

of the needle and noticed that during the traction period, the original actin flow on PLL substrate restored (Figure 2D). This indicates that the F-actin network in front of the adhesion site is uncoupled from the actin network, which is strongly coupled to the adhesion receptor under the needle tip.

We optimized the number of myosin motors n_m and the reinforcement constant k_{add0} at different substrate stiffnesses using experimental substrate deformation data corresponding to the time point when the actin retrograde flow decays to 20 nm/s (Figure 3; Supplemental Table 3). For the present study, we use the time when actin flow equals 20 nm/s as our new definition for latency time t_l for both experimental and modeling data, because our model does not provide any information about the time when the C domain starts to advance. The start of C domain advance was previously used as the experimental definition for latency time (Suter *et al.*, 1998). As shown in Figure 2D, the two time points of 20 nm/s actin flow and C domain advance are close together with C domain always advancing after actin flow has declined to 20 nm/s. The optimum n_m was estimated by rearranging the linear force-velocity equation (Equation 7). Here, we assigned a value of 6 pN for the motor stall force (F_s; Lohner *et al.*, 2019), and 100 nm/s for the unloaded actin flow rate (v_u), which corresponds to the actin flow rate of *Aplysia* growth cones grown on PLL (Lin and Forscher, 1995). From time-lapse recordings of ConA needle experiments, we determined the amount of substrate deformation x_{sub} at latency time t_l (Athamneh *et al.*, 2015). Once we estimated the optimum number of motors for each substrate stiffness, we optimized the reinforcement constant k_{add0} by running 40 simulations, where k_{add0} was assigned a value between 0.1 and 1. The sample mean and SD of the simulated latency time was estimated from each group of simulations. Lastly, the optimal value for k_{add0} at each substrate stiffness was chosen as the one for which the experimental latency time falls within one SD from the mean of the simulated time (Figure 3). When plotting the optimized number of myosin motors n_m and the optimized value of the reinforcement constant k_{add0} against substrate stiffness (Figure 3), the number of motors increases linearly with substrate stiffness, whereas k_{add0} exhibits a bimodal dependence on substrate stiffness. Specifically, the reinforcement constant increases from 0.2 at 2.5 pN/nm to 1 at 4 pN/nm, decreases to 0.2 at 14 pN/nm and increases subtly to 0.5 and 0.36 at 53 pN/nm and 106 pN/nm, respectively. This suggests that at a substrate stiffness of 4 pN/nm, clutch reinforcement has the largest effect on clutch efficacy.

Sensitivity analysis of latency time and substrate deformation

To test the robustness of our model around the optimized parameter space, we conducted a sensitivity analysis of the latency time t_l (Figure 4) and substrate deformation Δx_{sub} at that time (Figure 5) to changes of individual clutch and motor parameters as well as of combined parameters. The sensitivity of t_l and Δx_{sub} at this time for a specific parameter change is defined as the rate of change in t_l and Δx_{sub} per unit of change of a specific parameter. Figures 4 and 5 show the estimated output variable (t_l or Δx_{sub}) versus different parameter values for different substrate stiffness (left column), and the estimated sensitivity of output variable versus substrate stiffness for different parameter values (right column). The parameters can be divided into two groups according to their effects on t_l. For parameters such as the force threshold F_t (Figure 4B), the myosin stall force F_s (Figure 4C), the ratio k_{add0}/k_{on} (Supplemental Figure 3A), and the number of myosin motors n_m (Supplemental Figure 3C), t_l increases as the values of these parameter increase. The opposite can be observed for parameters such as the bond rupture force (Figure 4D), the ratio k_{on}/k_{off0} (Supplemental Figure 3B) and the number of clutches n_{c0} (Supplemental Figure 3E). Additionally, the latency time exhibits a biphasic dependence of the unloaded actin flow rate, being higher below or above the optimum value of 100 nm/s (Supplemental Figure 3D). When graphing latency time sensitivity against substrate stiffness for different parameters (Right column of Figure 4), we observed that below or above 4 pN/nm, the latency time is more sensitive to changes in the model parameters. However, at 4 pN/nm, the latency time is more stable, and the parameter space at which the system is mechanosensitive is wider. Thus, this might indicate that the optimum substrate stiffness for fast and efficient coupling in *Aplysia* growth cones is close to 4 pN/nm.

On the other hand, the substrate deformation Δx_{sub} at latency time is only sensitive to the motor-related parameters (Figure 5). In this case, the substrate deformation decreases if a specific parameter is below its optimized value and increases above this value. Furthermore, the estimated sensitivity of the substrate deformation for the motor-related parameters (Figure 5, right column), decreases when the substrate stiffness increases. This suggests that contrary to the findings for the latency time (Figure 4), the substrate deformation can be predicted only by the motor-related parameters, but similar to the latency time, it is differentially tuned across the parameter space at different substrate stiffness.

Comparing modeling with experimental data

To evaluate whether reinforcement by the number of bound clutches and of motors with increasing substrate stiffness reproduces the experimental substrate deformation behavior in our simulations, we compared simulated trajectories with and without adhesion reinforcement, and with different number of motors for a substrate stiffness of 4 pN/nm (Figure 6). As the number of motors increases, the amount of substrate deformation at equilibrium increases and the frequency of the load and fail cycles decreases, for both reinforced (Figure 6, A–C, left) and not reinforced simulations (Figure 6, A–C, right). However, the reinforcement takes the system from an unstable steady state (continuous oscillations) to a stable steady state (a constant substrate deformation), which corresponds to the adaptative behavior we observed experimentally (Athamneh *et al.*, 2015).

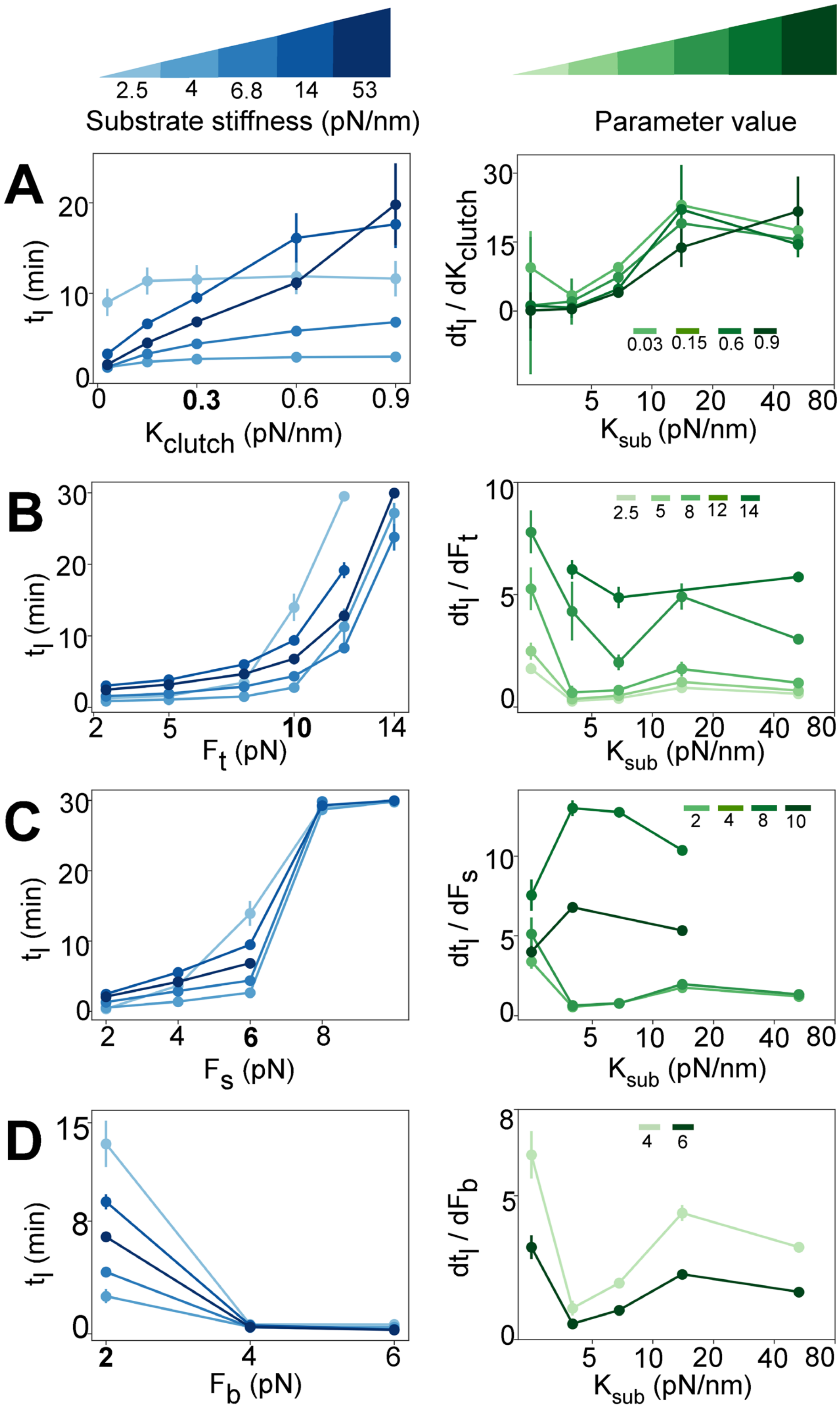

FIGURE 4: Sensitivity analysis of latency time. Left column: Estimated latency time (t_l) plotted versus different specific parameters at the experimental substrate stiffness (left color gradient). On each panel, the optimum value of the corresponding parameter is shown in bold, and for different values of the corresponding parameter the mean and SD from the mean is shown. Right column: Estimated sensitivity of the latency time plotted versus experimental substrate stiffness at different values (right color gradient) for the parameters, which are the same values shown in the x-axis of the corresponding figure in the left column. Moreover, t_l and sensitivity are shown only for the parameter values and substrate stiffness when the system is able to reach 20 nm/s, and each point corresponds to the average and standard deviations from simulations. The parameters are displayed from the highest to the lowest sensitivity of the latency time in the following order: A) Clutch spring constant (K_{clutch}) in pN/nm, (B) force threshold for adding a clutch (F_t) in pN, (C) Myosin stall force (F_s) in pN, (D) Bond rupture force (F_b) in pN. Sensitivity plots on the right are shown with a $\log_{10}$ scale for the x-axis. The rest of the parameters are shown in Supplemental Figure 3.

Lastly, we assessed our model by comparing our modeling results for latency time and substrate deformation versus substrate stiffness with our experimental data from microneedle experiments (Athamneh *et al.*, 2015; Figure 7). We found that the mean and standard deviations from $n = 40$ simulations at each substrate stiffness using the optimized parameters is in very good agreement with the experimental measurements (Figure 7, A and B). Consistent with the bimodal behavior observed for k_{add0} at low stiffness values between 2 and 14 pN/nm (Figure 3), the latency time showed the same trend but in opposite direction (Figure 7A). The latency time decreased from 14 min at 2.5 pN/nm to 2 min at 4 pN/nm and then increased at higher stiffness. The substrate deformation is the highest at lowest stiffness values (1.6 µm at 2.5 pN/nm) but then drops at higher substrate stiffness until it stabilizes around 0.8 µm. These results suggest that around 4 pN/nm substrate stiffness, the system is most effective in forming clutches; however, it stabilizes at stiffnesses higher than 14 pN/nm.

DISCUSSION

Chan and Odde (2008) developed a physical motor-clutch model that was validated with data derived from experiments with embryonic chick forebrain neurons growing on flexible substrates (Chan and Odde, 2008). This model predicts the retrograde actin flow rate and traction force of a single filopodium growing on a substrate with a specific stiffness. We previously used stiffness-calibrated microneedles to measure the substrate deformation produced by *Aplysia* growth cones and found that the substrate deformation and not the traction force is correlated with growth cone advance (Athamneh *et al.*, 2015). Here, we used these experimental data to modify the motor-clutch model with the following new features: an actin flow threshold of 20 nm/s, which indicates strong substrate-cytoskeletal coupling at latency time t_l; increasing number of motors n_m with increasing substrate stiffness; a clutch reinforcement constant k_{add0} that depends on substrate stiffness and clutch force; two new output variables called latency time t_l and the substrate deformation Δx_{sub}. After testing this model, we found that (1) the reinforcement constant is critical to reproduce the stiffness-dependent experimental latency time; (2) the reinforcement constant exhibits a bimodal dependence on the substrate stiffness (Figure 3), and is inversely proportional to the latency time (Figure 7A); (3) an increasing number of n_m is required with increasing substrate stiffness to reproduce the experimental substrate deformation at latency time (Figure 7); (4) the system is more robust to changes in the parameters, when the substrate stiffness is 4 pN/nm, which suggests that this stiffness could be close to the optimum.

The latency time is one of the new output variables of our modified motor-clutch model. We found very good agreement between experimental and simulated latency times as defined when actin flow drops to 20 nm/s (Figure 7A). The latency time initially decreases with increasing substrate stiffness, then increases, and finally stabilizes at 8 min for stiffer substrates. Conversely, the estimated reinforcement constant (k_{add0}) shows an opposite behavior (Figure 3). These results suggest that *Aplysia* growth cones respond faster to soft compared with stiff substrates, which is in agreement with findings with *Xenopus* retinal growth cones (Koser *et al.*, 2016). The amount of substrate deformation Δx_{sub} is the second new output from our revised motor-clutch model. Substrate deformation at latency time initially decreases with increasing substrate stiffness but then stabilizes at around 0.8–0.9 µm, when substrate stiffness is 4 pN/nm or higher (Figure 7B). Our findings on substrate deformation are in agreement with experiments conducted with silicon elastomers of different stiffness and epithelial cells or fibroblasts (Saez *et al.*, 2005; Ghibaudo *et al.*, 2008; Trichet *et al.*, 2012; Yip *et al.*, 2013). These studies report a linear increase in the traction force with stiffness, and a decrease in the substrate deformation with increasing substrate stiffness.

To address how latency time is affected by clutch- and motor-related parameters, we conducted a sensitivity analysis for several clutch-related parameters (Figure 4; Supplemental Figure 3). We found that the simulated latency time decreases when several clutch-related parameters increase to

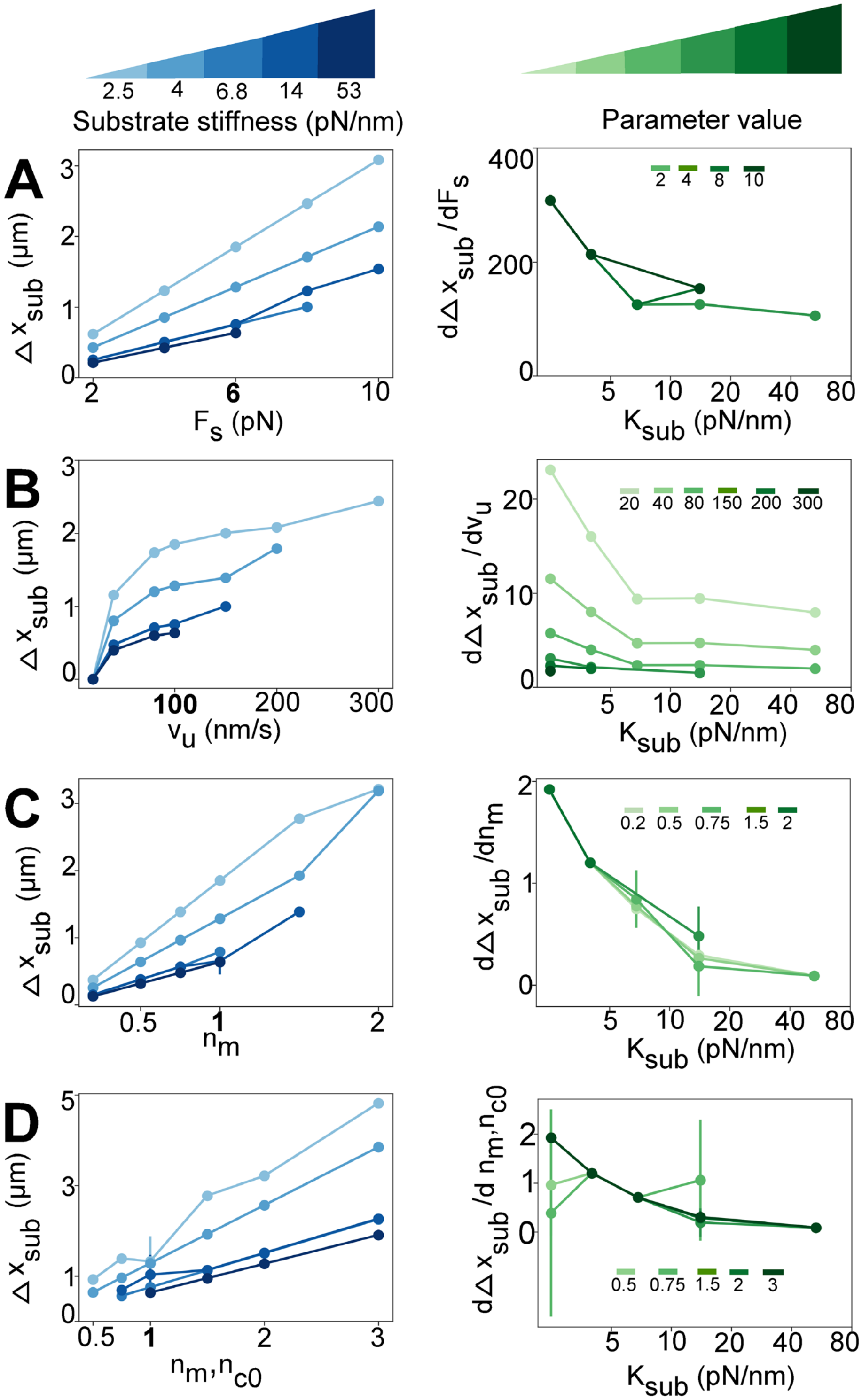

FIGURE 5: Sensitivity analysis of substrate deformation. Left column: Estimated substrate deformation at the latency time Δx_{sub} versus different specific parameters for a specific substrate stiffness (left color gradient). On each panel, the optimum value of the corresponding parameter is shown in bold, and for different values of the corresponding parameter the mean and SD from the mean is shown. Right column: Estimated sensitivity of the substrate deformation at the latency time versus experimental substrate stiffness at different values (right color gradient) for the parameters, which are the same values showed in the x axis of the corresponding figure in the left column. Moreover, Δx_{sub} and sensitivity are shown only for the parameter values and substrate stiffness when the system is able to reach 20 nm/s, and each point corresponds to the average and standard deviations from simulations. The parameters are displayed from the highest to the lowest sensitivity of Δx_{sub} in the following order: (A) Single myosin motor stall force (F_s) in pN, (B) unloaded actin flow velocity (v_u) in nm/s, (C) multiplication factor for number of myosin motors (n_m), (D) multiplication factor for number of myosin motors (n_m) and initial number of available clutches (n_{c0}). Sensitivity plots on the right are shown with a $\log_{10}$ scale for the x-axis.

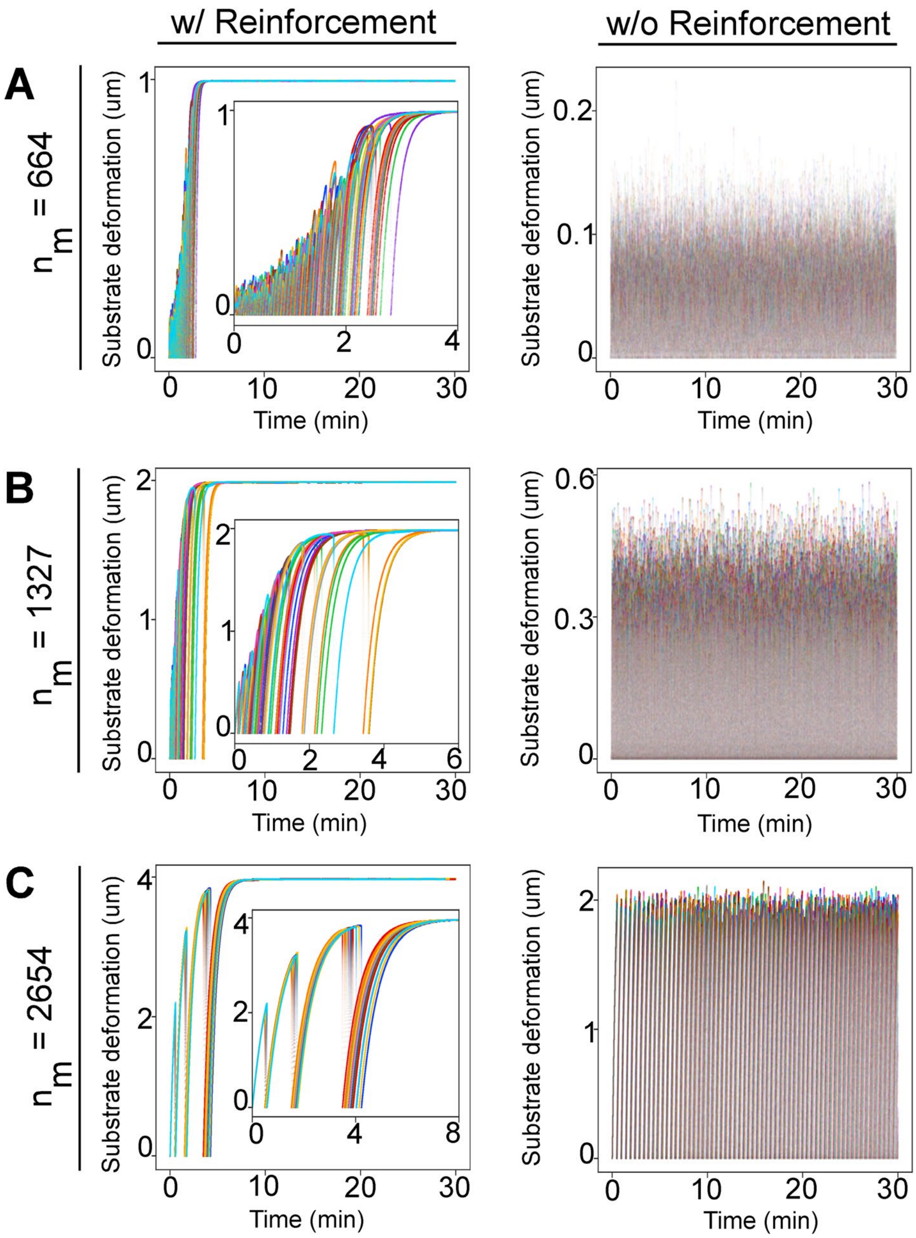

FIGURE 6: Effect of reinforcement and number of motors on the substrate deformation at 4 pN/nm. Substrate deformation Δx_{sub} vs time has been plotted for $n = 20$ simulation trajectories at 4pN/nm with the optimized parameters (Figure 3) and a specific number of motors. (A) Simulations with and without reinforcement with 664 motors. (B) Simulations with and without reinforcement with 1327 motors. (C) Simulations with and without reinforcement with 2654 motors.

strengthen the adhesions. For example, by increasing the bond rupture force, the ratio kon/koff or the number of clutches, the simulated latency time decreases. Similarly, when the actomyosin contractility decreases either by lowering the number of motors or the myosin stall force, the latency time decreases. These findings suggest that reinforcing the clutches will shorten the response time to acquire strong coupling, whereas increasing the number of myosins will have opposite effects, likely by increasing the time of each cycle (Figure 6). Additionally, the estimated sensitivity of the latency time to changes in either clutch or motor parameters is the lowest at 4 pN/nm substrate stiffness, which may indicate that 4 pN/nm represents the optimum stiffness for *Aplysia* growth cones. Adhesion reinforcement is necessary to reach a stable substrate deformation over time (Figure 6); without adhesion reinforcement, the system remains in a high-frequency oscillatory behavior from the beginning of the simulation. The oscillatory substrate deformation behavior was also observed in the experimental needle displacement data, although the extent of the oscillation was not the same.

What are the underlying molecular mechanisms of adhesion reinforcement? There is evidence for force-dependent adhesion strengthening in non-neuronal cells. When fibronectin-coated beads were restrained on fibroblasts using an optical tweezer, the integrin-cytoskeleton link was strengthened in proportion to the applied force by recruiting additional integrins to the adhesion site (Choquet *et al.*, 1997; Roca-Cusachs *et al.*, 2009). Adhesion molecules such as P-selectin can display catch bond behavior (Marshall *et al.*, 2003), which could explain reinforcement; however, so far, we do not have any evidence that the interaction between apCAM and ConA or F-actin involves any catch bonds. Another known reinforcement mechanism is the recruitment of cytoskeletal coupling proteins like talin and vinculin, which can undergo conformational changes upon stretching. This results in exposing cryptic binding sites to other proteins or phosphorylation sites, leading to the recruitment of additional proteins or activation of signaling cascades that contribute to further adhesion reinforcement. In this case, the recruitment of additional proteins is itself force-dependent, as shown for in vivo talin stretching experiments, where forces between 5 and 10 pN unfold the molecule and expose binding sites for vinculin (Yao *et al.*, 2016). Downstream activation of different signaling cascades during focal adhesion assembly and maturation allows the cell to fine tune the adhesion strength and contractility. Nichol and colleagues (2019) showed that RhoA signaling and phosphorylation of signaling enzymes are essential for the tensional homeostasis of human motor neurons grown on compliant substrates. Specifically, this study showed that on stiff substrates, there is an elevated level of phosphorylated FAK, Src and p130-CAS, as well as an elevated activity of RhoA, ROCK, myosin light chain, and myosin II (Nichol *et al.*, 2019). This is in agreement with the role of RhoA/ROCK pathway in regulating the myosin II contractility, where RhoA activates ROCK, and this in turn, phosphorylates myosin light chain and activates myosin II (Loudon *et al.*, 2006; Graessl *et al.*, 2017). Furthermore, it has been shown with embryonic rat hippocampal neurons that paxillin acts as a bistable switch that controls neurite initiation in a substrate stiffness-dependent manner (Chang *et al.*, 2017). Specifically, on soft substrates (0.1 kPa), paxillin is preferentially associated with endocytic vesicles, whereas on stiff substrates (20 kPa), paxillin is

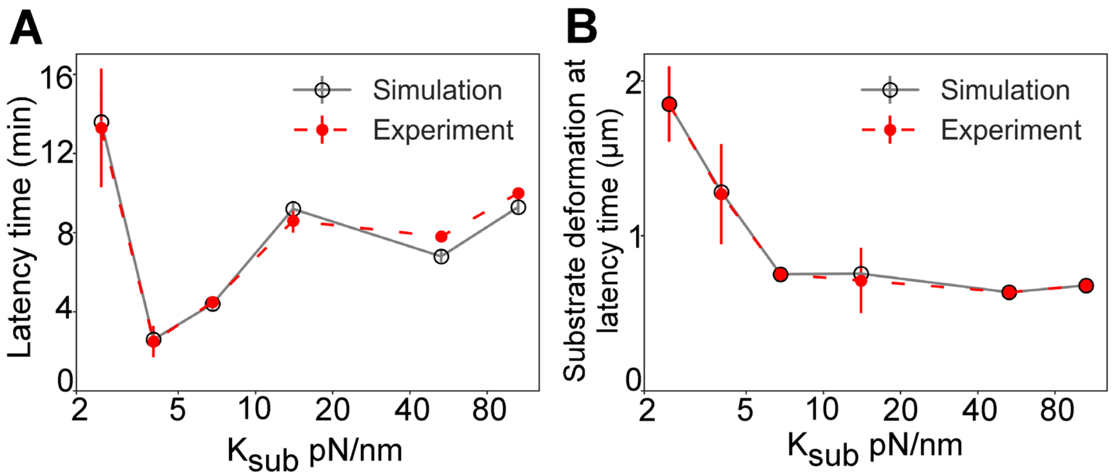

FIGURE 7: Comparison of experimental and simulation results. (A) Comparison of experimental and simulation results for the latency time t_l versus substrate stiffness K_{sub}. (B) Comparison of experimental and simulations results for the substrate deformation Δx_{sub} at latency time versus substrate stiffness K_{sub}. The number of experiments used for the optimization was $n = 2$ for 2.5 pN/nm, 4 pN/nm, and 14 pN/nm, and $n = 1$ for the rest of substrate stiffnesses. Thus, for the substrate stiffness with $n = 2$, the filled circles correspond to the average of the average of simulations optimized with each experiment, and the bars corresponds to the SD. x-axis is shown on a $\log_{10}$ scale.

mainly associated with focal adhesions via binding to vinculin (Chang *et al.*, 2017). Additionally, in hippocampal neurons grown on 0.1 kPa hydrogels coated with brain-derived growth factor, there is an increased paxillin-drebrin interaction in the T-zone, which is related to force generation and preferential growth cone turning on soft substrates (Chen *et al.*, 2022). In our model, the force is equally shared among all bound clutches, so adding more clutches contributes to increasing the adhesion lifetime by reducing the load on each clutch. It is known that not only the substrate stiffness but also the force-loading rate affect the cellular mechanosensitivity (Cui *et al.*, 2015; Oria *et al.*, 2017; Andreu *et al.*, 2021). Therefore, studying the effect of cyclic extracellular forces on growth cone migrations could provide additional information to unveil the molecular mechanism underlying growth cone mechanosensing.

In contrast to the latency time, the substrate deformation at latency time depends only on the motor-related parameters (Figure 5). Briefly, the substrate deformation exhibits an increasing linear trend across the parameter space (Figures 5 and 6). Increasing number of NMII motors with stiffness is essential to reproduce the experimental substrate deformation behavior at different substrate stiffnesses. Moreover, the estimated sensitivity of substrate deformation to motor-related parameters decreases as the substrate stiffness increases. These findings suggest that the growth cone needs to recruit more myosins when the substrate becomes stiffer. Without such a motor reinforcement mechanism, the system oscillates and does not reach a stable value (Figure 6). Although challenging, quantifying the number of active NMII motors could provide supportive evidence for the idea of myosin recruitment with increasing substrate stiffness.

There is evidence for force-dependent changes in myosin-F-actin interactions. All myosin motors undergo a mechanochemical cycle in which the force generation is coupled with ATP hydrolysis and structural changes associated with myosin-F-actin interactions (Houdusse and Sweeney, 2016). It is known that myosin II exhibits a load-dependent ADP release, which affects the time the myosin is bound to F-actin (duty ratio) and the fraction of bound or unbound myosin molecules (Kovács *et al.*, 2007). Additionally, micropipette aspiration experiments in *Dictystelium discoideum* showed a sigmoidal increase of myosin II at the site of force application, and that as the applied force increases, myosin II increases monotonically (Luo *et al.*, 2013). This behavior was simulated by a multiscale model of a myosin bipolar filament assembly, which considers a force-dependent myosin unbinding from F-actin and cooperativity among bound myosin molecules (Luo *et al.*, 2012; Schiffhauer *et al.*, 2019; Grewe and Schwarz, 2020). On the other hand, simulations using a two state cross-bridge model showed that the force output from the myosin ensemble in response to an external stiffness, depends on two variables: 1) the time of force buildup, and 2) time for which the myosin is attached to F-actin (Stam *et al.*, 2015). Specifically, this study showed that different myosin isoforms can respond differently to external stiffness. For example, NMIIA exhibits a sharp transition in both the time of force build up and time of F-actin attachment as stiffness increases suggesting that NMIIA is an adaptable motor.

In addition to the role of load-dependent kinetics on the myosin force output, the compliance of different actin crosslinkers, the structure of the actin network, and interfilamentous spacing also influence the force output (Weirich *et al.*, 2021; Muresan *et al.*, 2022). For example, by comparing experimental data of myosin motion with simulations, it was found that as the interfilamentous spacing increases, the number of myosin heads required to produce a specific force increase. Moreover, for a specific number of myosin heads, the force output increases with the crosslinker stiffness or the compliance of the actin network (Weirich *et al.*, 2021). Taken together, several previous studies suggest that changes in the structure and dynamics of the actomyosin cytoskeleton can fine-tune the myosin force output spatiotemporally. Because the myosin dynamics in our motor-clutch model is simple, it could be interesting to explore the effects of a more complex and dynamic actomyosin system on the substrate deformation in our model.

We have revised the motor-clutch model by adding a reinforcement feature at the level of both clutches and motors as well as a threshold for actin flow speed, which indicates the transition from weak to strong coupling. The new outputs of the model – latency time and substrate deformation – reproduce the experimental data of the mechanosensitive response of *Aplysia* growth cones very well. Latency time is shortened by strengthening adhesions and reducing the number of myosins, whereas the amount substrate deformation is only sensitive to motor-related parameters. Our results suggest that a substrate stiffness of 4 pN/nm is optimal for *Aplysia* growth cones to acquire a strong coupling state in minimal time. In conclusion, our findings indicate that *Aplysia* growth cones appear to prefer soft over stiff substrates when given the choice.

MATERIALS AND METHODS

Request a protocol through *Bio-protocol*.

Aplysia bag cell neuronal culture

Aplysia bag cell neurons were collected from the abdominal ganglion as described previously (Lee *et al.*, 2008), and cultured on a glass bottom dish (Fluorodish Cell Culture Dish, World Precision Instruments, Sarasota, FL) coated with 20 ug/ml PLL and immersed in L15 medium supplemented with artificial sea water (ASW; 400 mM NaCl; 9 mM $CaCl_2$; 27 mM $MgSO_4$; 28 mM $MgCl_2$; 4 mM L-glutamine; 50 mg/ml gentamicin; 5 mM HEPES, pH 7.9). After plating, the cells were kept at 14°C and typically used for experiments 1 d after plating.

Preparation and calibration of microneedles

Microneedles were prepared as described in Athamneh *et al.* (2015). In brief, microneedles were prepared by pulling 5 µl glass capillaries (Drummond Scientific, Broomall, PA) using a Narishige PP-832 vertical micropipette puller (Narishige, East Meadow, NY). The settings on the puller were modified to get a tapered tip, which was brought close to puller heater to ensure a smooth round tip. Subsequently, microneedle stiffness was measured using a laser Doppler vibrometer (LDV) according to Lozano *et al.* (2010). We used a Polytec MSA-400 scanning LDV (Polytec Gmbh, Waldbronn, Germany) to measure thermal vibration time series at the tip of the microneedle. The incident beam of the interferometer (wavelength λ = 633 nm; power <1 mW; 1 mm spot size) was focused through a 50x microscope objective. Later, the power spectral density of velocity time series was estimated using Welch's periodogram method, and the first flexural resonance was fitted to a single harmonic oscillator. Those parameters were used to calculate the stiffness of the microneedle as previously described in Lozano *et al.* (2010) by using a script written in MATLAB version 2013a (The Math-Works, Natick, MA)

Measuring growth cone traction force using stiffness-calibrated microneedles

Stiffness-calibrated microneedles were cleaned in piranha solution (H_2SO_4:H_2O_2 = 3:1) for 20 min, rinsed five times in distilled water, and incubated in 100 µg/ml Con A (Vector Laboratories, Burlingame, CA) in TBS. We used a three-dimensional (3D)-hydraulic micromanipulator (Narishige, East Meadow, NY) to position the microneedle on the growth cone P domain between the leading edge and the T zone. When the needle tip was in contact with the growth cone, time-lapse DIC imaging was performed using a Nikon TE2000 E2 Eclipse (Nikon, Melville, NY) inverted microscope with a 60 × 1.4 NA oil immersion DIC objective (plus additional 1.5x magnification) and a Cascade II charge-coupled device camera (Photometrics, Tucson, AZ) controlled by MetaMorph software version 7.8.6 (Molecular Devices, Sunnyvale, CA). Images were acquired every 10 s after the microneedle was placed in contact with the growth cone and until the C domain reached the microneedle tip.

Data analysis

The microneedle displacement along the x and y axis was measured using the ImageJ plugin TrackMate. The detection algorithm was Difference of Gaussians, and filters for the spot quality and x and y positions were used, so the needle tip was detected as a single circular object per frame. Additionally, measurements of the actin retrograde flow in front and behind the microneedle, as well as the velocities of the boundaries corresponding to the C and P domains, were obtained from kymographs using the MetaMorph 7.8.6 kymograph tool after processing the time lapse DIC movies in the following order: a 4 × 4 low pass filter, a Laplace filter, and a 3 × 3 low pass filter. All data were saved as csv files, and the corresponding time series were plotted in Python 3.8.

Implementation of motor-clutch model

The simulations were run in Python 3.8. The time evolution of the motor-clutch model was simulated using the direct method of the stochastic simulation algorithm (Gillespie, 1977). Briefly, three types of reaction with corresponding rates are considered: clutch binding (k_{on}), clutch unbinding (k_{off}), and clutch reinforcement (k_{add}). Each reaction j has a parameter c_j that can be either k_{on}, k_{off}, or k_{add}, and a parameter h_j that represents the number of molecules that participate in the reaction. In our study, h_j is equal to 1, because we consider only unimolecular reactions. Each time step was calculated using a uniform random number (r_1) between [0, 1] and the sum of all reaction probabilities through the following equation:

$$\Delta t = \frac{-ln(r_1)}{\sum_{j=1}^{3} h_j c_j} = \frac{-ln(r_1)}{\sum_{j=1}^{3} c_j} \quad (1)$$

Then, the time was advanced by Δt:

$$t_k = t_{k-1} + \Delta t \quad (2)$$

where k is an index that describes the number of simulated events and takes a value between 0 and the total number of simulated events for a specific set of parameters. For each simulation, the number of simulated events depends on the time required to reach the latency time.

After the time step was calculated, the second random number (r_2) was drawn uniformly from [0, 1]. A reaction j is executed in the next time step, if r_2 is equal or greater than the quotient between the probability of each reaction and the sum of all reaction probabilities as follows:

$$\frac{c_j}{\sum_{j=1}^{3} c_j} \le r_2 \quad (3)$$

The physical behavior of the motor-clutch system was modeled using the model proposed by Chan and Odde (2008), and the reinforcement equation proposed by Mekhdjian and colleagues (Mekhdjian *et al.*, 2017). The model workflow is shown in Supplemental Figure 2, and the parameter values as well as variable abbreviations are shown in the Supplemental Tables 1 and 2.

During each simulation event, we defined a variable i to represent each clutch. Because the number of available clutches at each time step changes due to the reinforcement, i can take any value between 1 and $n_c(t_k)$, which is the total number of available clutches at time k. Assuming that each clutch and the substrate can be represented as elastic springs, the force on each clutch ($F_{clutch(i)}$; Equation 4) was calculated using the clutch spring constant (K_{clutch}), the clutch position ($x_i(t_{k-1})$) and the substrate position ($x_{sub}(t_{k-1})$) at the previous time step:

$$F_{clutch(i)}(t_k) = K_{clutch} * \left(x_i(t_{k-1}) - x_{sub}(t_{k-1})\right) \quad (4)$$

Next, unbound clutches were allowed to bind F-actin with a fixed binding rate k_{on} (Supplemental Table 1), bound clutches unbind from F-actin with a force-dependent unbinding rate $k_{off(i)}$ (Equation 5) using the Bell model (Bell, 1978), and the adhesion reinforcement rate k_{add} was calculated using Equation 6.

$$k_{off(i)}(t_k) = k_{off0} * e^{\left(\frac{F_{clutch(i)}(t_k)}{F_b}\right)} \quad (5)$$

$$k_{add}(t_k) = k_{add0} * \left(\sum_{i=1}^{n_{eng}} a_{(i)}(t_k)\right) * f_{available}(t_k) \quad (6)$$

In Equation 6, k_{add} represents the rate at which new clutches are added to the system. k_{add0} is the optimized rate for each substrate stiffness, n_{eng} is the number of engaged clutches at time t_k, and $a_{(i)}$ is 1 or 0 depending on whether or not the force on clutch is greater than a force threshold F_t:

$$a_{(i)}(t_k) = \begin{cases} 1 & if \quad F_{clutch(i)}(t_k) \geq F_t \\ 0 & if \quad F_{clutch(i)}(t_k) < F_t \end{cases}$$

and, $f_{available}(t)$ is the fraction of available clutches for reinforcement:

$$f_{available}(t_k) = \frac{n_{c,max} - n_c(t_k)}{n_{c,max}}$$

$n_{c,max}$ and n_c are the maximum allowed number of clutches in the system and the number of available clutches at time t_k, respectively.

One of the three reactions was chosen according to Equation 3, and the time was advanced as stated in Equation 2. Consequentially, the clutch state was updated accordingly, and the retrograde actin flow ($v_f(t_k)$; Equation 7), the clutch position ($x_i(t_k)$; Equation 8) and the substrate position ($x_{sub}(t_k)$; Equation 9) were calculated as follows:

$$v_f(t_k) = v_u * \left(1 - \frac{K_{sub} * x_{sub}(t_{k-1})}{n_m * F_s}\right) \quad (7)$$

$$x_i(t_k) = x_i(t_{k-1}) + v_f(t_k) * \Delta t \quad (8)$$

$$x_{sub}(t_k) = \frac{K_{clutch} * \sum_{i=1}^{n_{eng}} x_i(t_k)}{K_{sub} + n_{eng} * K_{clutch}} \quad (9)$$

Sensitivity analysis

Individual and combined parameter sensitivities were estimated using a finite-difference scheme known as the common random numbers approach (Rathinam *et al.*, 2010), which uses the same two random numbers to simulate the system with the optimum parameter set and with a change in one of the parameters. Thus, the sensitivities of the substrate deformation and the latency time to a change h in a specific parameter, was estimated dividing the difference between the perturbed and unperturbed variables by h. Furthermore, we used a custom-written script in Python 3.8 to calculate the sample mean and SD of the sensitivity estimate, the latency time, and the substrate deformation at latency.

Code availability

The code will be made available upon request.

ACKNOWLEDGMENTS

This work was supported by funding from National Science Foundation (1146944-IOS) and National Institutes of Health (5R01NS117701).

REFERENCES

Abe K, Katsuno H, Toriyama M, Baba K, Mori T, Hakoshima T, Kanemura Y, Watanabe R, Inagaki N (2018). Grip and slip of L1-CAM on adhesive substrates direct growth cone haptotaxis. Proc Natl Acad Sci 115, 2764–2769.

Andreu I, Falcones B, Hurst S, Chahare N, Quiroga X, Le Roux A-L, Kechagia Z, Beedle AEM, Elosegui-Artola A, Trepat X, *et al.* (2021). The force loading rate drives cell mechanosensing through both reinforcement and cytoskeletal softening. Nat Commun 12, 4229.

Athamneh AIM, Cartagena-Rivera AX, Raman A, Suter DM (2015). Substrate deformation predicts neuronal growth cone advance. Biophys J 109, 1358–1371.

Bangasser BL, Rosenfeld SS, Odde DJ (2013). Determinants of maximal force transmission in a motor-clutch model of cell traction in a compliant microenvironment. Biophys J 105, 581–592.

Bard L, Boscher C, Lambert M, Mege R-M, Choquet D, Thoumine O (2008). A molecular clutch between the actin flow and N-cadherin adhesions drives growth cone migration. J Neurosci 28, 5879–5890.

Bell GI (1978). Models for the specific adhesion of cells to cells: A theoretical framework for adhesion mediated by reversible bonds between cell surface molecules. Science 200, 618–627.

Burnette DT, Ji L, Schaefer AW, Medeiros NA, Danuser G, Forscher P (2008). Myosin II activity facilitates microtubule bundling in the neuronal growth cone neck. Dev Cell 15, 163–169.

Chan CE, Odde DJ (2008). Traction dynamics of filopodia on compliant substrates. Science 322, 1687–1691.

Chang T-Y, Chen C, Lee M, Chang Y-C, Lu C-H, Lu S-T, Wang D-Y, Wang A, Guo C-L, Cheng P-L (2017). Paxillin facilitates timely neurite initiation on soft-substrate environments by interacting with the endocytic machinery. eLife 6, e31101.

Chen C, Chu C-H, Chu Y, Chang T-Y, Chen S-W, Liang S-Y, Tsai Y-C, Chen B-C, Tu H-L, Cheng P-L (2022). Neuronal paxillin and drebrin mediate BDNF-induced force transduction and growth cone turning in a soft-tissue-like environment. Cell Rep 40, 111188.

Choquet D, Felsenfeld DP, Sheetz MP (1997). Extracellular matrix rigidity causes strengthening of integrin–cytoskeleton linkages. Cell 88, 39–48.

Cui Y, Hameed FM, Yang B, Lee K, Pan CQ, Park S, Sheetz M (2015). Cyclic stretching of soft substrates induces spreading and growth. Nat Commun 6, 6333.

Dent EW, Gertler FB (2003). Cytoskeletal dynamics and transport in growth cone motility and axon guidance. Neuron 40, 209–227.

Elosegui-Artola A, Bazellieres E, Allen MD, Andreu I, Oria R, Sunyer R, Gomm JJ, Marshall JF, Jones JL, Trepat X, Roca-Cusachs P (2014). Rigidity sensing and adaptation through regulation of integrin types. Nat Mater 13, 7.

Elosegui-Artola A, Oria R, Chen Y, Kosmalska A, Pérez-González C, Castro N, Zhu C, Trepat X, Roca-Cusachs P (2016). Mechanical regulation of a molecular clutch defines force transmission and transduction in response to matrix rigidity. Nat Cell Biol 18, 540–548.

Flanagan LA, Ju Y-E, Marg B, Osterfield M, Janmey PA (2002). Neurite branching on deformable substrates. Neuroreport 13, 2411–2415.

Franze K, Gerdelmann J, Weick M, Betz T, Pawlizak S, Lakadamyali M, Bayer J, Rillich K, Gögler M, Lu Y-B, *et al.* (2009). Neurite branch retraction is caused by a threshold-dependent mechanical impact. Biophys J 97, 1883–1890.

Georges PC, Miller WJ, Meaney DF, Sawyer ES, Janmey PA (2006). Matrices with compliance comparable to that of brain tissue select neuronal over glial growth in mixed cortical cultures. Biophys J 90, 3012–3018. https://doi.org/10.1529/biophysj.105.073114

Ghibaudo M, Saez A, Trichet L, Xayaphoummine A, Browaeys J, Silberzan P, Buguin A, Ladoux B (2008). Traction forces and rigidity sensing regulate cell functions. Soft Matter 4, 1836.

Gillespie DT (1977). Exact stochastic simulation of coupled chemical reactions. J Phys Chem 81, 2340–2361.

Graessl M, Koch J, Calderon A, Kamps D, Banerjee S, Mazel T, Schulze N, Jungkurth JK, Patwardhan R, Solouk D, *et al.* (2017). An excitable Rho GTPase signaling network generates dynamic subcellular contraction patterns. J Cell Biol 216, 4271–4285.

Grewe J, Schwarz US (2020). Mechanosensitive self-assembly of myosin II minifilaments. Phys Rev E 101, 022402.

Houdusse A, Sweeney HL (2016). How myosin generates force on actin filaments. Trends Biochem Sci 41, 989–997.
Koch D, Rosoff WJ, Jiang J, Geller HM, Urbach JS (2012). Strength in the periphery: Growth cone biomechanics and substrate rigidity response in peripheral and central nervous system neurons. Biophys J 102, 452–460.
Koser DE, Thompson AJ, Foster SK, Dwivedy A, Pillai EK, Sheridan GK, Svoboda H, Viana M, Costa LDF, Guck J, *et al*. (2016). Mechanosensing is critical for axon growth in the developing brain. Nat Neurosci 19, 1592–1598.
Kostic A, Sap J, Sheetz MP (2007). RPTPα is required for rigidity-dependent inhibition of extension and differentiation of hippocampal neurons. J Cell Sci 120, 3895–3904.
Kovács M, Thirumurugan K, Knight PJ, Sellers JR (2007). Load-dependent mechanism of nonmuscle myosin 2. Proc Natl Acad Sci 104, 9994–9999.
Lee AC, Decourt B, Suter DM (2008). Neuronal cell cultures from Aplysia for high-resolution imaging of growth cones. J Vis Exp 12, 662.
Lin C-H, Forscher P (1995). Growth cone advance is inversely proportional to retrograde F-actin flow. Neuron 14, 763–771.
Lohner J, Rupprecht J-F, Hu J, Mandriota N, Saxena M, De Araujo DP, Hone J, Sahin O, Prost J, Sheetz MP (2019). Large and reversible myosin-dependent forces in rigidity sensing. Nat Phys 15, 689–695.
Loudon RP, Silver LD, Yee Jr. HF, Gallo G (2006). RhoA-kinase and myosin II are required for the maintenance of growth cone polarity and guidance by nerve growth factor. J Neurobiol 66, 847–867.
Lowery LA, Vactor DV (2009). The trip of the tip: Understanding the growth cone machinery. Nat Rev Mol Cell Biol 10, 332–343.
Lozano JR, Kiracofe D, Melcher J, Garcia R, Raman A (2010). Calibration of higher eigenmode spring constants of atomic force microscope cantilevers. Nanotechnology 21, 465502.
Luo T, Mohan K, Srivastava V, Ren Y, Iglesias PA, Robinson DN (2012). Understanding the cooperative interaction between myosin II and actin cross-linkers mediated by actin filaments during mechanosensation. Biophys J 102, 238–247.
Luo T, Mohan K, Iglesias PA, Robinson DN (2013). Molecular mechanisms of cellular mechanosensing. Nat Mater 12, 1064–1071.
Marshall BT, Long M, Piper JW, Yago T, McEver RP, Zhu C (2003). Direct observation of catch bonds involving cell-adhesion molecules. Nature 423, 190–193.
Medeiros NA, Burnette DT, Forscher P (2006). Myosin II functions in actin-bundle turnover in neuronal growth cones. Nat Cell Biol 8, 216–226.
Mekhdjian AH, Kai F, Rubashkin MG, Prahl LS, Przybyla LM, McGregor AL, Bell ES, Barnes JM, DuFort CC, Ou G, *et al*. (2017). Integrin-mediated traction force enhances paxillin molecular associations and adhesion dynamics that increase the invasiveness of tumor cells into a three-dimensional extracellular matrix. Mol Biol Cell 28, 1467–1488.
Miller KE, Suter DM (2018). An integrated cytoskeletal model of neurite outgrowth. Front Cell Neurosci 12, 447.
Mitchison T, Kirschner M (1988). Cytoskeletal dynamics and nerve growth. Neuron 1, 761–772.
Muresan CG, Sun ZG, Yadav V, Tabatabai AP, Lanier L, Kim JH, Kim T, Murrell MP (2022). F-actin architecture determines constraints on myosin thick filament motion. Nat Commun 13, 7008.
Nichol RH, Hagen KM, Lumbard DC, Dent EW, Gómez TM (2016). Guidance of axons by local coupling of retrograde flow to point contact adhesions. J Neuros 36, 2267–2282.
Nichol RH, Catlett TS, Onesto MM, Hollender D, Gómez TM (2019). Environmental elasticity regulates cell-type specific RHOA signaling and neuritogenesis of human neurons. Stem Cell Rep 13, 1006–1021.
Oria R, Wiegand T, Escribano J, Elosegui-Artola A, Uriarte JJ, Moreno-Pulido C, Platzman I, Delcanale P, Albertazzi L, Navajas D, *et al*. (2017). Force loading explains spatial sensing of ligands by cells. Nature 552, 219–224.
Rathinam M, Sheppard PW, Khammash M (2010). Efficient computation of parameter sensitivities of discrete stochastic chemical reaction networks. J Chem Phys 132, 034103.
Robles E, Gomez TM (2006). Focal adhesion kinase signaling at sites of integrin-mediated adhesion controls axon pathfinding. Nat Neurosci 9, 1274–1283.
Roca-Cusachs P, Gauthier NC, Del Rio A, Sheetz MP (2009). Clustering of α5β1 integrins determines adhesion strength whereas αvβ3 and talin enable mechanotransduction. Proc Natl Acad Sci 106,16245–16250.
Rosso G, Liashkovich I, Young P, Röhr D, Shahin V (2017). Schwann cells and neurite outgrowth from embryonic dorsal root ganglions are highly mechanosensitive. Nanomed Nanotechnol Biol Med 13, 493–501.
Saez A, Buguin A, Silberzan P, Ladoux B (2005). Is the mechanical activity of epithelial cells controlled by deformations or forces? Biophys J 89, L52–L54.
Santiago-Medina M, Gregus KA, Gomez TM (2013). PAK–PIX interactions regulate adhesion dynamics and membrane protrusion to control neurite outgrowth. J Cell Sci 126, 1122–1133.
Santos TE, Schaffran B, Broguière N, Meyn L, Zenobi-Wong M, Bradke F (2020). Axon growth of CNS neurons in three dimensions is amoeboid and independent of adhesions. Cell Rep 32, 107907.
Schiffhauer ES, Ren X, Iglesias VA, Kothari P, Iglesias PA, Robinson DN (2019). Myosin IIB assembly state determines its mechanosensitive dynamics. J Cell Biol 218, 895–908.
Spedden E, Wiens MR, Demirel MC, Staii C (2014). Effects of surface asymmetry on neuronal growth. PLoS One 9, e106709.
Stam S, Alberts J, Gardel ML, Munro E (2015). Isoforms confer characteristic force generation and mechanosensation by myosin II filaments. Biophys J 108, 1997–2006.
Stoeckli ET (2018). Understanding axon guidance: Are we nearly there yet? Development 145, dev151415.
Suter DM, Errante LD, Belotserkovsky V, Forscher P (1998). The Ig superfamily cell adhesion molecule, apCAM, mediates growth cone steering by substrate–cytoskeletal coupling. J Cell Biol 141, 227–240.
Suter DM, Forscher P (2000). Substrate–cytoskeletal coupling as a mechanism for the regulation of growth cone motility and guidance. J Neurobiolo 44, 97–113.
Suter DM, Forscher P (2001). Transmission of growth cone traction force through apCAM–cytoskeletal linkages is regulated by Src family tyrosine kinase activity. J Cell Biol 155, 427–438.
Tanaka A, Fujii Y, Kasai N, Okajima T, Nakashima H (2018). Regulation of neuritogenesis in hippocampal neurons using stiffness of extracellular microenvironment. PLoS One 13, e0191928.
Thompson C, Lin C-H, Forscher P (1996). An Aplysia cell adhesion molecule associated with site-directed actin filament assembly in neuronal growth cones. J Cell Sci 109, 2843–2854.
Toriyama M, Kozawa S, Sakumura Y, Inagaki N (2013). Conversion of a signal into forces for axon outgrowth through Pak1-mediated Shootin1 phosphorylation. Curr Biol 23, 529–534.
Trichet L, Le Digabel J, Hawkins RJ, Vedula SRK, Gupta M, Ribrault C, Hersen P, Voituriez R, Ladoux B (2012). Evidence of a large-scale mechanosensing mechanism for cellular adaptation to substrate stiffness. Proc Natl Acad Sci 109, 6933–6938.
Weirich KL, Stam S, Munro E, Gardel ML (2021). Actin bundle architecture and mechanics regulate myosin II force generation. Biophys J 120, 1957–1970.
Yamashita M (2015). Weak electric fields serve as guidance cues that direct retinal ganglion cell axons in vitro. Biochem Biophys Rep 4, 83–88.
Yao M, Goult BT, Klapholz B, Hu X, Toseland CP, Guo Y, Cong P, Sheetz MP, Yan J (2016). The mechanical response of talin. Nat Commun 7, 11966.
Yip AK, Iwasaki K, Ursekar C, Machiyama H, Saxena M, Chen H, Harada I, Chiam K-H, Sawada Y (2013). Cellular response to substrate rigidity is governed by either stress or strain. Biophys J 104, 19–29.
Zhang X-F, Schaefer AW, Burnette DT, Schoonderwoert VT, Forscher P (2003). Rho-dependent contractile responses in the neuronal growth cone are independent of classical peripheral retrograde actin flow. Neuron 40, 931–944.